*Progress In Electromagnetics Research C, Vol. 96, 205–214, 2019*

# Enhanced Power Transmission for On-Road AGV Wireless Charging Systems Using a Current-Optimized Technique

**Jin Zhang[1, 2, 4, *], Dong Chen[2, 3], and Chen Zhang[2, 3]**

**Abstract**—This paper provides a sound wireless power transfer (WPT) recharging solution for on-road automated guided vehicle (AGV) system. In this solution, multiple transmitting coils serve as power transmitters (TXs), and a receiving coil in AGV serves as a power receiver (RX). The multiple TXs are along a straight track for dynamic charging to AGV. The circuit model of multiple-TX and single-RX WPT system is first constructed based on circuit theory (CT), and then current-optimized scheme based on Lagrangian multiplier method is proposed to tune the currents in multiple TXs to maximize the power delivered to the load (PDL). The equal current (EC Case) flowing through each TX is compared with the optimal current (OC Case). Through contrastive analysis, the OC Case shows its advantages in PDL. Finally, the theoretical analysis results are confirmed by the results of full-wave electromagnetic simulation.

## 1. INTRODUCTION

Wireless power transfer (WPT) technology based on magnetic coupling was proposed by Nicola Tesla a century ago [1]. With a great potential for application and the maturity of power electronics for providing high-frequency power supply, WPT has achieved a rapid progress in recent decades.

The early structure of a magnetic coupling WPT system was composed of four elements: source loop, transmitting coil (TX), receiving coil (RX), and load loop [2–4]. In order to heighten transmission distance with power delivered to the load (PDL), multi-repeater WPT systems have been proposed [5–8]. The practical application of a single charging platform supplying power to multiple devices attracts a great deal of attention [9–11], and some approaches using multiple TXs to transfer more power to a single RX have been studied in [12–14].

Methodologically, much early literature focused on magnetic resonance WPT using pure physical method known as coupled-mode theory (CMT) [2, 5, 15]. In recent years, circuit theory (CT) has become the primary means of analyzing the magnetic resonance WPT system due to tangible electrical parameters used in this theory. The technologies shaping the magnetic flux in a steerable beam based on CT have been developed in multiple-TX systems [16–18]. The theory of the maximum system efficiency in proportional to the radiation efficiency of the transmitting and receiving antenna has been found and verified in radiating near-field region of antennas [19–21].

All the above-mentioned references have spurred rapid progress in WPT technology. Of course, a suitable system structure and an analytical method need to be chosen according to different application scenarios. Automated guided vehicles (AGVs) have been widely applied in scenes like storage logistics, smart manufacturing, and port transportation. Manual charging old battery, replacing the dead battery

*Received 27 July 2019, Accepted 19 October 2019, Scheduled 3 November 2019*

* Corresponding author: Jin Zhang (jinzhang@jit.edu.cn).

[1] School of Electronic and Information Engineering, Jinling Institute of Technology, Nanjing 211169, People's Republic of China. [2] National and Local Joint Engineering Laboratory of RF Integration and Micro-Assembly Technology, Nanjing 210023, People's Republic of China. [3] School of Electric Science and Engineering, Nanjing University of Posts and Telecommunications, Nanjing 210023, People's Republic of China. [4] School of Electrical Engineering, Southeast University, Nanjing 210096, People's Republic of China.

with a full battery and contact auto-charge are at present the main AGV charging methods. With the sustainable growth of AGV, the original power supply modes led to higher operating costs and lower productivities. In order to solve the problems of the mainstream charging means mentioned above, WPT technology is introduced to recharge AGV automatically [22–24]. In [22], in order to avoid the power loss caused by the side offset of RX to TX, the positioning tolerance is improved by optimizing the coil and ferrite geometry of TX and RX using the FEM method. Reference [23] focuses on an RFID-enabled positioning system for AGVs, which can be used to realize a perfect alignment of TX and RX in a WPT system to maximize wireless charging efficiency. An interoperable power adjustment mechanism for AGV on-road wireless charging is presented in [24]. The method of mapped impedance acting as an indicator to sense the dynamic location of that moving AGV is proposed in this reference. However, to our knowledge, previous researches focused on the schemes of coil positioning and improving the offset tolerance between TXs and RX. The optimal method for maximizing PDL under limited transmitters and feeding power is absent.

In this paper, the scenario of on-road AGV wireless charging application shown in Fig. 1(a) is investigated using circuit theory. The receiving coil mounted in a vehicle is marked as RX, and multiple feeding transmitters marked as $TX_i$ $(i = 1, \cdots, n)$ are arranged along a straight track where the AGV moves on. Fig. 1(b) illustrates the equivalent circuit model of the on-road WPT system of Fig. 1(a). This paper is organized as follows. The circuit model and optimal approaches of the proposed multiple-TX WPT system are presented in Section 2. In this section, the analysis and comparison of two cases of equal and optimal current (EC and OC Case) are illustrated to highlight the superiority of the current-optimized methodology. In Section 3, the results of the theoretical calculation are executed by MATLAB, and full-wave electromagnetic simulation is carried out by FEKO software to validate the theoretical calculation. Finally, Section 4 contains some concluding remarks.

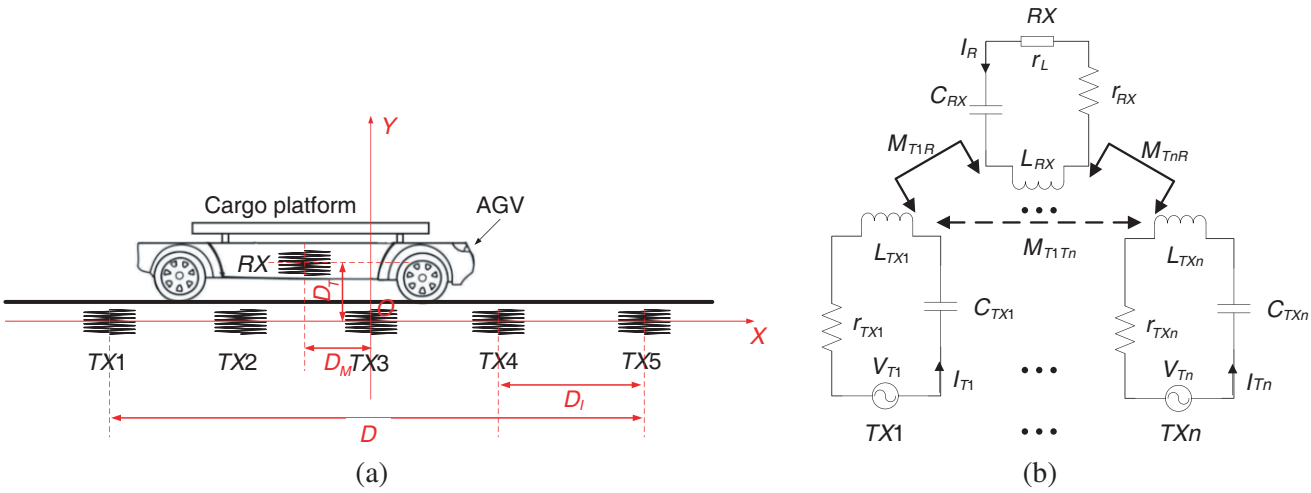


**Figure 1.** (a) Multiple-TX WPT system for AGV charging. (b) Circuit topology of the proposed multiple-TX WPT system.

## 2. MODEL AND OPTIMIZATION OF MULTIPLE-TX WPT

According to Kirchhoff's circuit laws, the electrical properties for the multi-TX WPT system in Fig. 1(b) can be described by the following formula:

$$\begin{bmatrix} \frac{1}{r'_{RX}} \begin{bmatrix} r_{TX1} & j\omega_0 M_{T1T2} & \cdots & j\omega_0 M_{T1Tn} \\ j\omega_0 M_{T1T2} & r_{TX2} & \cdots & j\omega_0 M_{T2Tn} \\ \vdots & \vdots & \vdots & \ddots \\ j\omega_0 M_{T1Tn} & j\omega_0 M_{T2Tn} & \cdots & r_{TXn} \end{bmatrix} & \begin{matrix} -jQ_{T1R} \\ -jQ_{T2R} \\ \vdots \\ -jQ_{TnR} \end{matrix} \\ \begin{matrix} -jQ_{T1R} & -jQ_{T2R} & \cdots & -jQ_{TnR} \end{matrix} & 1 \end{bmatrix} \begin{bmatrix} \mathbf{I_{T1}} \\ \mathbf{I_{T2}} \\ \vdots \\ \mathbf{I_{Tn}} \\ \mathbf{I_R} \end{bmatrix} = \frac{1}{r'_{RX}} \begin{bmatrix} \mathbf{V_{T1}} \\ \mathbf{V_{T2}} \\ \vdots \\ \mathbf{V_{Tn}} \\ \mathbf{0} \end{bmatrix} \quad (1)$$

where $M_{TiTj}$ $(i, j = 1, \cdots, n, i \neq j)$ is the mutual inductance between $TX_i$ and $TX_j$; $V_{Ti}$, $I_{Ti}$, and $r_{TXi}$ are the source voltage, loop current, and parasitic resistance of $TX_i$, respectively; $I_R$ and $r'_{RX}$ are the loop current and total resistance of $RX$. $r'_{RX}$ can be written as $r'_{RX} = r_{RX} + r_L$, where $r_{RX}$ and $r_L$ are the parasitic resistance of $RX$ and the resistance of the load. $Q_{TiR} = \omega_0 M_{TiR}/r'_{RX}$ is defined as transmission quality factor, where $\omega_0$ and $M_{TiR}$ are the resonance frequency and the mutual inductance between $TX_i$ and $RX$, respectively. It can be found that $Q_{TiR}$ indicates the coupling strengths when $RX$ and load are fixed.

The first $n$ lines and the last line of Equation (1) can be written in Equations (2a) and (2b), respectively, as follows:

$$r_{TXi}\mathbf{I_{Ti}} + j\omega_0 \sum_{j=1, j\neq i}^{n} (M_{TiTj}\mathbf{I_{Tj}}) - r'_{RX} j Q_{TiR}\mathbf{I_R} = \mathbf{V_{Ti}} \tag{2a}$$

$$\mathbf{I_R} - j\sum_{i=1}^{n} (Q_{TiR}\mathbf{I_{Ti}}) = 0 \tag{2b}$$

The $PDL$ for the multi-TX WPT system, $PDL = r_L |\mathbf{I_R}|^2$, can be achieved via Eq. (2b)

$$PDL = r_L \left( \sum_{i=1}^{n} Q_{TiR}\mathbf{I_{Ti}} \right)^2 \tag{3}$$

$\mathbf{V_{Ti}}$ can be expressed explicitly in terms of $\mathbf{I_{Ti}}$ using equations of Eqs. (2a) and (2b). The power gained from the $i$-th source, $P_{TXi}$, is calculated by $P_{TXi} = \mathrm{Re}(\mathbf{V_{Ti}}\mathbf{I^*_{Ti}})$.

$$P_{TXi} = \left( r_{TXi} + r'_{RX} Q^2_{TiR} \right) |\mathbf{I_{Ti}}|^2 + \omega_0 Q_{TiR} \sum_{j=1, j\neq i}^{n} M_{TjR}\mathbf{I_{Tj}}\mathbf{I_{Ti}} \tag{4}$$

The detailed calculation of total feeding power to the WPT network, $P_{TX} = \sum_{i=1}^{n} P_{TXi}$, is as follows:

$$P_{TX} = \sum_{i=1}^{n} r_{TXi}\mathbf{I^2_{Ti}} + r'_{RX} \left( \sum_{i=1}^{n} Q_{TiR}\mathbf{I_{Ti}} \right)^2 \tag{5}$$

For a traditional multiple-TX WPT system, equal current (EC Case) flows through each TX. The identical current, $\mathbf{I_{T,I}}$, can be derived from Equation (5)

$$\mathbf{I_{T,I}} = \frac{\sqrt{P_{TX}}}{\sqrt{\sum_{i=1}^{n} r_{TXi} + r'_{RX} \left( \sum_{i=1}^{n} Q_{TiR} \right)^2}} \tag{6}$$

Combining Equations (3) and (6), $PDL$ for a conventional multiple-TX system with identical currents in TXs is derived in Equation (7)

$$PDL_I = \frac{P_{TX} r_L}{r'_{RX} + \frac{1}{F_1}} \tag{7}$$

where $F_1 = \left(\sum_{i=1}^{n} Q_{TiR}\right)^2 / \sum_{i=1}^{n} r_{TXi}$

In order to maximize $PDL$ via optimizing $\mathbf{I_{Ti}}$ in each TX under the equality constraint of Eq. (5), we achieve optimized objective functions as follows.

$$\max_{\mathbf{I_{Ti}}} PDL\left(\mathbf{I_{Ti}}\right) : \; r_L \left( \sum_{i=1}^{n} Q_{TiR}\mathbf{I_{Ti}} \right)^2 \tag{8a}$$

$$\text{s.t.} \; \sum_{i=1}^{n} r_{TXi}\mathbf{I^2_{Ti}} + r'_{RX} \left( \sum_{i=1}^{n} Q_{TiR}\mathbf{I_{Ti}} \right)^2 - P_{TX} = 0 \tag{8b}$$

The optimal solutions of $\mathbf{I_{Ti,\,OPT}}$ for Eq. (8) could be obtained by using the Lagrangian multiplier method. Introducing variable, $\lambda$, in a set of real numbers the optimization of Eq. (8) is constructed by Lagrange multiplier equation:

$$L\left(\mathbf{I_{Ti}},\lambda\right)=r_L\left(\sum_{i=1}^{n}Q_{TiR}\mathbf{I_{Ti}}\right)^2+\lambda\left[\sum_{i=1}^{n}r_{TXi}\mathbf{I}_{\mathbf{Ti}}^2+r'_{RX}\left(\sum_{i=1}^{n}Q_{TiR}\mathbf{I_{Ti}}\right)^2-P_{TX}\right] \tag{9}$$

The necessary conditions of optimal solutions for Eq. (9) are $\nabla_{\mathbf{I_{Ti}}}L(\mathbf{I_{Ti}},\lambda)=0$ and $\nabla_{\lambda}L(\mathbf{I}_{Ti},\lambda)=0$, whose corresponding expansions are listed as follows:

$$\mathbf{I_{Ti}}=\frac{Q_{TiR}\left(r_L-r'_{RX}\lambda\right)}{\lambda r_{TXi}}\left(\sum_{j=1}^{n}Q_{TjR}\mathbf{I_{Tj}}\right) \tag{10a}$$

$$\sum_{i=1}^{n}r_{TXi}\mathbf{I}_{\mathbf{Ti}}^2+r'_{RX}\left(\sum_{i=1}^{n}Q_{TiR}\mathbf{I_{Ti}}\right)^2-P_{TX}=0 \tag{10b}$$

From Eq. (10a), the relations of current flowing in different loops are deduced of $\mathbf{I_{Ti}}/\mathbf{I_{Tj}}=(Q_{TiR}/r_{TXi})/(Q_{TjR}/r_{TXj})$, $\forall i\neq j$. Substituting the relations of $\mathbf{I_{Ti}}/\mathbf{I_{Tj}}$ into Eq. (10b), the optimal current (OC Case) in the $i$-th TX, $\mathbf{I_{Ti,\,OPT}}$, is:

$$\mathbf{I_{Ti,\,OPT}}=\frac{\sqrt{P_{TX}}Q_{TiR}\left(\prod_{j=1,\,j\neq i}^{n}r_{TXj}\right)}{\sqrt{\left[\sum_{s=1}^{n}Q_{TsR}^2\left(\prod_{j=1,\,j\neq s}^{n}r_{TXj}\right)\right]\left\{\prod_{j=1}^{n}r_{TXj}+r'_{RX}\left[\sum_{s=1}^{n}Q_{TsR}^2\left(\prod_{j=1,\,j\neq s}^{n}r_{TXj}\right)\right]\right\}}} \tag{11}$$

By substituting $\mathbf{I_{Ti,OPT}}$ of Eq. (11) into Eq. (3), one can derive the optimal $PDL$ of multi-TXs, $PDL_{OPT}$.

$$PDL_{OPT}=\frac{P_{TX}r_L}{r'_{RX}+\frac{1}{F_2}} \tag{12}$$

where $F_2=\sum_{i=1}^{n}\left(Q_{TiR}^2/r_{TXi}\right)$.

Comparing $PDL_I$ of EC Case in Equation (7) and the optimal $PDL_{OPT}$ of OC Case in Equation (12) for a multi-TX system, the only difference lies in $F_1$ and $F_2$. To order to compare the numeric value of $PDL_I$ and $PDL_{OPT}$, $\Delta F=F_2-F_1$ is implemented as follows:

$$\Delta F=\frac{\sum_{i=1,\,i\neq j}^{n}\left[\left(Q_{TiR}r_{TXj}-Q_{TjR}r_{TXi}\right)^2\left(\prod_{s=1,\,s\neq i,\,\neq j}^{n}r_{TXs}\right)\right]}{\left(\sum_{i=1}^{n}r_{TXi}\right)\left(\prod_{i=1}^{n}r_{TXi}\right)} \tag{13}$$

There are many groups of $Q_{TiR}r_{TXj}\neq Q_{TjR}r_{TXi}$ for different sizes of the loop in a multi-TX system; therefore, $\Delta F>0$ is always tenable. Up to this point, the conclusion that the value of $PDL_{OPT}$ of the proposed multi-TX system with current-controlled technique must be greater than that of $PDL_I$ of a conventional multi-TX system with the identical feeding current is true.

## 3. THEORETICAL CALCULATION AND FULL-WAVE ELECTROMAGNETIC SIMULATION VERIFICATION

To verify the effectiveness of the optimal method for maximizing the PDL in a multiple-TX WPT system, a WPT system with a maximum of five identical TXs and a single RX is modeled in this section. The

dimension parameters of TX and RX are: the coil diameters of TX and RX are $d_{TX} = d_{RX} = 0.31\,\text{m}$; the numbers of turns of TX and RX are $T_{TX} = T_{RX} = 25$; a 1.2-mm diameter copper wire with electrical conductivity of $5.7 \times 10^7\,\text{S/m}$ is used to wind the power transmission coils. The electrical parameters of the WPT system calculated according to theory are: the self-inductance values of TX and RX are $L_{TX} = L_{RX} = 40.55\,\mu H$; the lumped capacitors of capacitance values of $C_{TX} = C_{RX} = 625\,\text{pF}$ are connected to TX and RX coils in series respectively to achieve the resonance frequency $f_0 = 1\,\text{MHz}$ ($\omega_0 = 6.28 \times 10^6\,\text{rad/s}$); the parasitic resistance values of the TX and RX coils are $r_{TXi} = r_{RX} = 1.96\,\Omega$; the load resistance is $r_L = 100\,\Omega$. The relative positions of the TX and RX coils are shown in Fig. 1(a). The total charging interval between $TX_1$ and $TX_5$ is $D = 2\,\text{m}$. The distances between two adjacent TXs are identical and set as $D_I = 0.5\,\text{m}$, and the transmission distance $D_T$ changes from 0.1 m to 0.7 m. The maximum output power of the whole system is $P_{TX} = 30\,\text{W}$, which is allocated by the five TXs according to distinct optimization goals.

For 5-TX system, the transmission quality factor $Q_{TiR}$ can be obtained for different range shift $D_M$ by calculating the $M_{TiR}$ and the known $\omega_0$ and $r'_{RX}$. The identical current, $\mathbf{I_{T,I}}$, in EC Case for the traditional multiple-TX WPT system and the optimal current, $\mathbf{I_{Ti,OPT}}$, in OC Case for maximizing the PDL system are calculated by MATLAB using the expressions in Equations (6) and (11), respectively. Figs. 2(a) and (b) show the current amplitude values of $\mathbf{I_{T,I}}$ and $\mathbf{I_{Ti,OPT}}$ versus $D_M$ at two transfer distances of $D_T = 0.2$ and 0.5 m, respectively. $\mathbf{I_{Ti,OPT}}$ is symmetrical about the position of $TX_i$. By comparing Figs. 2(a) and (b), it can be found that both $\mathbf{I_{Ti,OPT}}$ and $\mathbf{I_{T,I}}$ increase along with the increase of $D_T$. The reason is that the increasing current can maintain stable feeding power with increasing $D_T$. Both of the fluctuation ranges of $\mathbf{I_{T,I}}$ and $\mathbf{I_{Ti,OPT}}$ decrease with the increase of $D_T$.

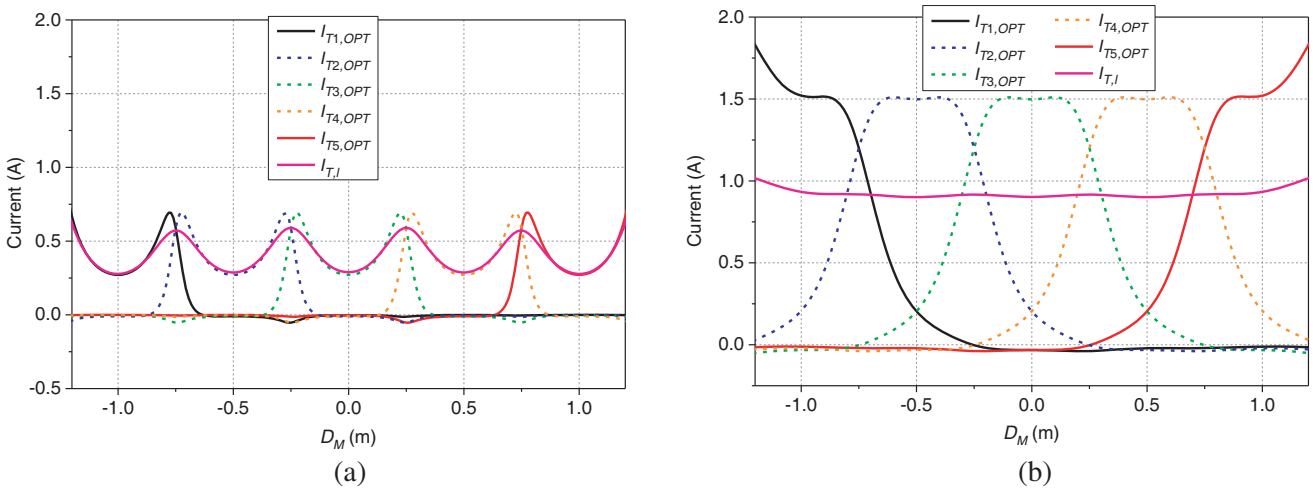


**Figure 2.** Calculated current values for EC and OC Cases in 5-TX AGV charging system, (a) $D_T = 0.2\,\text{m}$; (b) $D_T = 0.5\,\text{m}$.

In practice, the voltage source is more commonly used to feed power than the current source, and voltage source can only serve as the feeding source for wire port in FEKO, which is a comprehensive computational electromagnetics (CEM) software and is used as a means of verification in this paper. The feeding voltages of $\mathbf{V_{Ti}}$ and $\mathbf{V_{Ti,OPT}}$ for the $PDL_I$ and $PDL_{OPT}$ can be achieved by substituting $\mathbf{I_{T,I}}$ and $\mathbf{I_{Ti,OPT}}$ into Equation (2), respectively. The $i$th voltage feeding to $TX_i$ is written as:

$$\mathbf{V_{Ti}} = r_{TXi}\mathbf{I_{T,I}} + r'_{RX}Q_{TiR}\sum_{j=1}^{n} Q_{TjR}\mathbf{I_{T,I}} + j\omega_0 \sum_{j=1,j\neq i}^{n} M_{TiTj}\mathbf{I_{T,I}} \tag{14a}$$

$$\mathbf{V_{Ti,OPT}} = r_{TXi}\mathbf{I_{Ti,OPT}} + r'_{RX}Q_{TiR}\sum_{j=1}^{n} Q_{TjR}\mathbf{I_{Tj,OPT}} + j\omega_0 \sum_{j=1,j\neq i}^{n} M_{TiTj}\mathbf{I_{Tj,OPT}} \tag{14b}$$

For the 5-TX system with $D_I = 0.5\,\text{m}$, $M_{TiTj}$ between $TX_i$ and $TX_j$ can be computed as

$$M_{TiTj}|_{\substack{i=1,\cdots,5\\ j=1,\cdots,5}} = \begin{bmatrix} M_{T1T1} & M_{T1T2} & M_{T1T3} & M_{T1T4} & M_{T1T5} \\ M_{T2T1} & M_{T2T2} & M_{T2T3} & M_{T2T4} & M_{T2T5} \\ M_{T3T1} & M_{T3T2} & M_{T3T3} & M_{T3T4} & M_{T3T5} \\ M_{T4T1} & M_{T4T2} & M_{T4T3} & M_{T4T4} & M_{T4T5} \\ M_{T5T1} & M_{T5T2} & M_{T5T3} & M_{T5T4} & M_{T5T5} \end{bmatrix}$$

$$= \begin{bmatrix} 0 & 3.6 & 0.38 & 0.11 & 0.04 \\ 3.6 & 0 & 3.6 & 0.38 & 0.11 \\ 0.38 & 3.6 & 0 & 3.6 & 0.38 \\ 0.11 & 0.38 & 3.6 & 0 & 3.6 \\ 0.04 & 0.11 & 0.38 & 3.6 & 0 \end{bmatrix} (\mu\text{H}) \quad (15)$$

The feeding voltage values of $\mathbf{V_{Ti}}$ and $\mathbf{V_{Ti,OPT}}$ are calculated using Equations (14) and (15). The magnitude and phase parts of the calculational results versus the position of RX, $D_M$, are shown in Fig. 3. For both cases in the figure, the maximum feeding voltage magnitude of the $i$-th transmitter, $TX_i$, appears when RX moves to the position right above $TX_i$. By comparing the OC Case in Figure 3(a) and EC Case in 3(b), the main differences are the voltage phase values between corresponding $TX_i$. Fig. 4 shows the magnitude and phase parts versus the positions of TXs for OC and EC Cases when RX is placed at two locations of $D_M = 0\,\text{m}$ and $-0.25\,\text{m}$. The voltages feeding to the five TXs are symmetric about the position of RX for the two Cases. The voltage values shown in Figs. 3 and 4 are used in FEKO to verify the theoretical optimization results in the following pages.

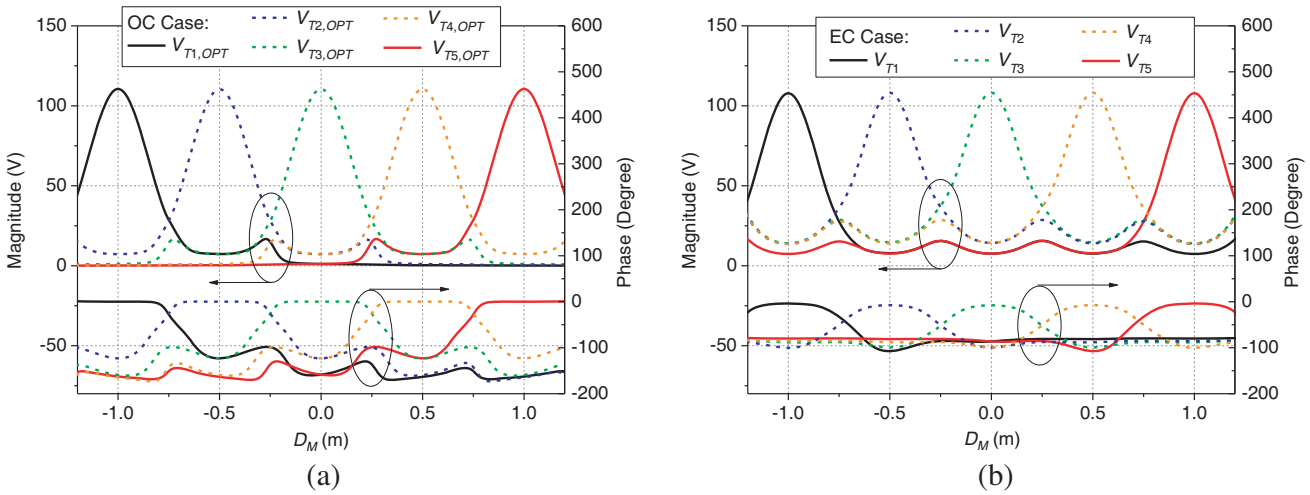


**Figure 3.** Feeding voltage values versus $D_M$ in 5-TX wireless charging system when $D_T = 0.2\,\text{m}$. (a) The magnitude and phase parts for OC Case; (b) the magnitude and phase parts for EC Case.

The calculated $PDL_I$ and $PDL_{OPT}$ using the identical and optimal currents for 5-TX WPT system are illustrated in Fig. 5. The scatter contour lines of the counterparts shown in Fig. 5 are obtained by FEKO simulation to verify the presented theory. The feeding voltage values of voltage sources shown in Figs. 3 and 4 are used in FEKO simulation. $PDL_I$ and $PDL_{OPT}$ versus $D_M$ are shown in Fig. 5(a). It can be found that $PDL_{OPT}$s in black lines are higher than $PDL_I$s in red lines over the whole research range from $D_M = -1.2\,\text{m}$ to $D_M = 1.2\,\text{m}$. The differences between $PDL_{OPT}$s and $PDL_I$s increase with the transmission distance of increasing $D_T$. Therefore, the advantages of the proposed optimization method are more obvious when $D_T$ is long. When the position of RX is fixed at $D_M = 0\,\text{m}$ and $= -0.25\,\text{m}$, PDLs versus $D_T$ are shown in Fig. 5(b). $PDL_{OPT}$s of OC Case in black lines are always greater than $PDL_I$s of EC Case in red lines at corresponding $D_M$. The PDL decreases gradually with increase of $D_T$ when $D_M = 0\,\text{m}$; however, the counterpart increases first and then decreases with increase of $D_T$

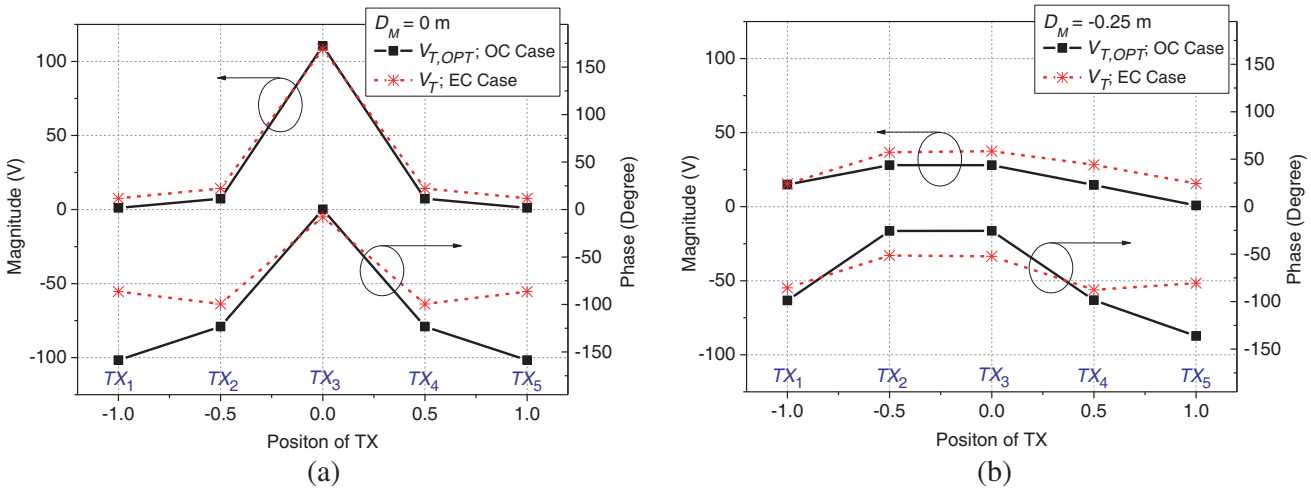


**Figure 4.** Feeding voltage values of OC and EC Cases versus the positions of TXs in 5-TX wireless charging system when $D_T = 0.2\,\text{m}$, (a) $D_M = 0\,\text{m}$, (b) $D_M = -0.25\,\text{m}$.

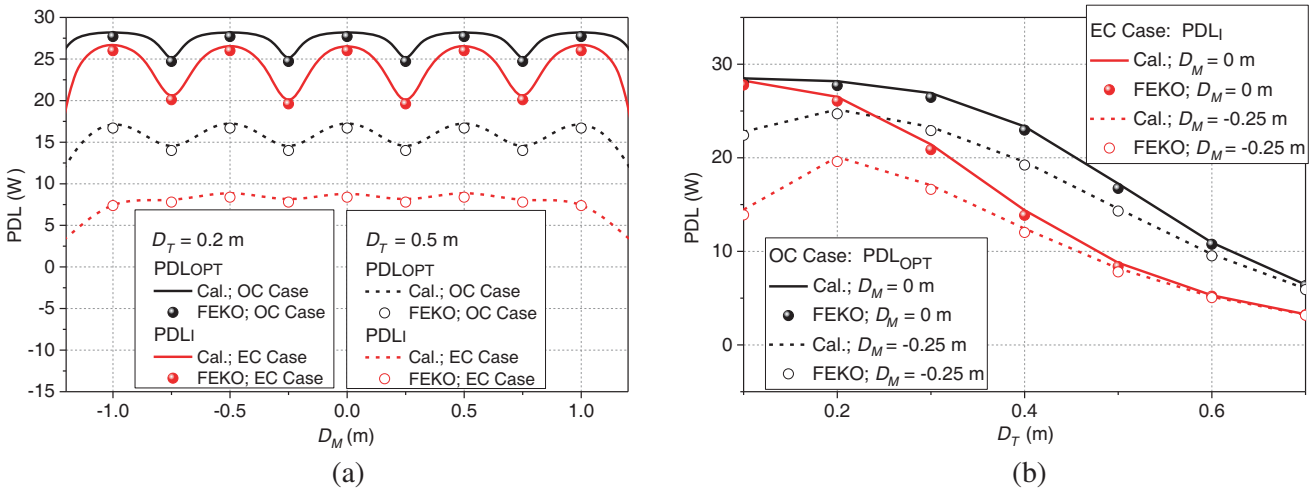


**Figure 5.** Simulated and calculated PDL of OC and EC Cases. (a) PDL values versus $D_M$ when $D_T = 0.2\,\text{m}$ and $0.5\,\text{m}$, (b) PDL values versus $D_T$ when $D_M = 0\,\text{m}$ and $-0.25\,\text{m}$.

when $D_M = -0.25\,\text{m}$. This is because the main power source is $TX_3$ at $D_M = 0\,\text{m}$, and the coupling coefficient between $TX_3$ and RX decreases gradually with increase of $D_T$. However, the main power feeding to RX is from two transmitters of $TX_2$ and $TX_3$ at $D_M = -0.25\,\text{m}$ case, and the coupling coefficients between the two TXs ($TX_2$ and $TX_3$) and RX are increased and then decreased with the increase of $D_T$ due to the offset placement of RX to $TX_2$ and $TX_3$. The simulated values shown in scatter contour lines match pretty well with the calculated values shown in solid lines in Fig. 5, which verifies the theoretical scheme and optimization method proposed in Section 2.

Based on Equations (14a) and (14b), the feeding voltage values of voltage sources for OC and EC Case are calculated for the five-TX wireless charging system. These voltage values are used in FEKO simulation to obtain the magnetic flux densities along the power transfer direction at $D_T = 0.2\,\text{m}$. Fig. 6 shows the simulation results in a setting plane which is perpendicular to the planes of coils. For $D_M = 0\,\text{m}$ case, $PDL_{OPT}$ and maximum axial magnetic field $H_{Y\,\max}$ of OC Case are higher than those of EC Case, and unlike OC Case, the magnetic flux density generated by each TX in EC Case is the same due to the identical emission current in each TX. For $D_M = -0.25\,\text{m}$ case, the same conclusion can be obtained. For OC Case, $H_{Y\,\max} = 225\,\text{A/m}$ at $D_M = -0.25\,\text{m}$ is higher than $H_{Y\,\max} = 100\,\text{A/m}$

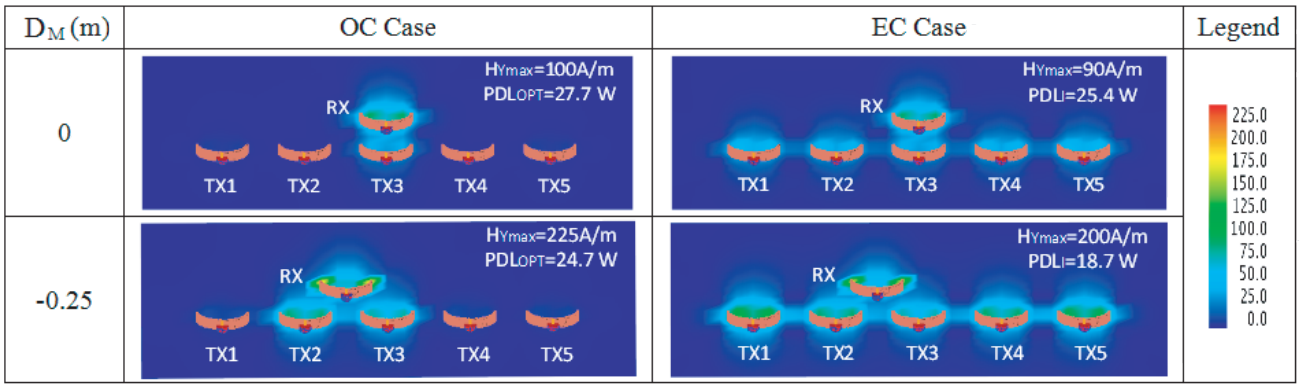


**Figure 6.** The distribution of magnetic fields of 5-TX wireless charging system when $D_T = 0.2\,\mathrm{m}$.

at $D_M = 0\,\mathrm{m}$; however, $PDL_{OPT} = 24.7\,\mathrm{W}$ at $D_M = -0.25\,\mathrm{m}$ is lower than $PDL_{OPT} = 27.7\,\mathrm{W}$ at $D_M = 0\,\mathrm{m}$. This is because each of the emission currents in $TX_2$ and $TX_3$ for $D_M = -0.25\,\mathrm{m}$ case is larger than that in $TX_3$ for $D_M = 0\,\mathrm{m}$ case (see Fig. 2(a)). The maximum magnetic flux density of $D_M = -0.25\,\mathrm{m}$ case exists around $TX_2$ and $TX_3$; however, the power delivered to RX is still lower than that of $D_M = 0\,\mathrm{m}$ case. For EC Case, the similar conclusion that $H_{Y\,\max}$ ($PDL_{OPT}$) at $D_M = -0.25\,\mathrm{m}$ is higher (lower) than that at $D_M = 0\,\mathrm{m}$ is still valid. The same reason as OC Case can be used to clarify this similar conclusion.

## 4. CONCLUSIONS

In this paper, under the application background of on-road AGV wireless charging, the scheme of multiple-TX wireless charging is presented. The multiple TXs are lined along the AGV track to realize on-move recharging.

The multiple-TX WPT system is theoretically analyzed based on circuit theory. The optimal current solution of assigning currents at different TXs is proposed to maximize the PDL when the number of TXs is fixed. By contrast, the equal current case is presented to illustrate the advantages of the proposed optimal solution. The current parameters mapping to the corresponding voltage values of feeding sources are implemented. Based on the electromagnetic simulation software FEKO, the three-dimensional full-wave simulation is implemented using the transformation feeding voltage values to verify the optimization solution.

This paper provides a sound WPT recharging solution for a moving AGV using a multiple-TX system when the TXs are in linear arrangement.

## ACKNOWLEDGMENT

This research was supported in part by the Natural Science Foundation of the Jiangsu Higher Education Institutions of China(Grant No. 19KJB510029), the open research fund of the National and Local Joint Engineering Laboratory of RF Integration and Micro-Assembly Technology (KFJJ20180203), the Joint Funds of the National Natural Science Foundation of China (U1636108), the Scientific Research Foundation for the High-Level Talents of Jinling Institute of Technology (jit-b-201719), and the Scientific Research Incubation Foundation of Jinling Institute of Technology (jit-fhxm-201802). Jin Zhang would like to thank Dr. Dong Chen for helpful discussions for improving this paper.

## REFERENCES

1. Tesla, N., "Apparatus for transmitting electrical energy," U.S. Patent 1 119 732, Dec. 1, 1914.

2. André, K., K. Aristeidis, M. Robert, J. D. Joannopoulos, F. Peter, and S. Marin, "Wireless power transfer via strongly coupled magnetic resonances," *Science*, Vol. 317, 83–86, 2007.
3. Sample, A. P., D. T. Meyer, and J. R. Smith, "Analysis, experimental results, and range adaptation of magnetically coupled resonators for wireless power transfer," *IEEE Transactions on Industrial Electronics*, Vol. 58, 544–554, 2011.
4. Zhang, J. and C. Cheng, "Quantitative investigation into the use of resonant magneto-inductive links for efficient wireless power transfer," *IET Microwaves Antennas & Propagation*, Vol. 10, 38–44, 2016.
5. Zhang, F., S. A. Hackworth, W. Fu, C. Li, Z. Mao, and M. Sun, "Relay effect of wireless power transfer using strongly coupled magnetic resonances," *IEEE Transactions on Magnetics*, Vol. 47, 1478–1481, 2011.
6. Ahn, D. and S. Hong, "A study on magnetic field repeater in wireless power transfer," *IEEE Transactions on Industrial Electronics*, Vol. 60, 360–371, 2013.
7. Zhong, W., C. K. Lee, and S. Y. R. Hui, "General analysis on the use of Tesla's resonators in domino forms for wireless power transfer," *IEEE Transactions on Industrial Electronics*, Vol. 60, 261–270, 2013.
8. Zhang, J. and C. Cheng, "Analysis and optimization of three-resonator wireless power transfer system for predetermined-goals wireless power transmission," *Energies*, Vol. 9, 274, 2016.
9. Fu, M., Z. Tong, C. Ma, and X. Zhu, "Efficiency and optimal loads analysis for multiple-receiver wireless power transfer systems," *IEEE Transactions on Microwave Theory & Techniques*, Vol. 63, 801–812, 2015.
10. Fu, M., H. Yin, M. Liu, Y. Wang, and C. Ma, "A 6.78 MHz multiple-receiver wireless power transfer system with constant output voltage and optimum efficiency," *IEEE Transactions on Power Electronics*, Vol. 33, 5330–5340, 2018.
11. Hao, P., L. Lu, and Z. Liang, "Priority evaluation for multiple receivers in wireless power transfer based on magnetic resonance," *2016 IEEE Wireless Power Transfer Conference (WPTC)*, 1–4, 2016.
12. Zhang, J. and F. Wang, "Efficiency analysis of multiple-transmitter wireless power transfer systems," *International Journal of Antennas and Propagation*, Vol. 2018, 11, 2018.
13. Zhang, C., D. Lin, and S. Y. Hui, "Basic control principles of omnidirectional wireless power transfer," *IEEE Transactions on Power Electronics*, Vol. 31, 5215–5227, 2016.
14. Johari, R., J. V. Krogmeier, and D. J. Love, "Analysis and practical considerations in implementing multiple transmitters for wireless power transfer via coupled magnetic resonance," *IEEE Transactions on Industrial Electronics*, Vol. 61, 1774–1783, 2013.
15. Kiani, M. and M. Ghovanloo, "The circuit theory behind coupled-mode magnetic resonance-based wireless power transmission," *IEEE Transactions on Circuits and Systems I: Regular Papers*, Vol. 59, 2065–2074, 2012.
16. Jadidian, J. and D. Katabi, "Magnetic MIMO: How to charge your phone in your pocket," *International Conference on Mobile Computing and Networking*, 495–506, 2014.
17. Moghadam, M. R. V. and R. Zhang, "Node placement and distributed magnetic beamforming optimization for wireless power transfer," *IEEE Transactions on Signal and Information Processing over Networks*, Vol. 4, 264–279, 2018.
18. Yang, G., M. R. V. Moghadam, and R. Zhang, "Magnetic beamforming for wireless power transfer," *2016 IEEE International Conference on Acoustics, Speech and Signal Processing (ICASSP)*, 3936–3940, 2016.
19. Lee, J. and S. Nam, "Fundamental aspects of near-field coupling small antennas for wireless power transfer," *IEEE Transactions on Antennas and Propagation*, Vol. 58, 3442–3449, 2010.
20. Zhang, J. and C. Cheng, "Investigation of near-field wireless power transfer between two efficient electrically small planar antennas," *2014 IEEE 3rd Asia-Pacific Conference on Antennas and Propagation (APCAP)*, 720–723, 2014.

21. Chen, Z., H. Sun, and W. Geyi, "Maximum wireless power transfer to the implantable device in the radiative near field," *IEEE Antennas and Wireless Propagation Letters*, Vol. 16, 1780–1783, 2017.
22. Daniel, K., C. Rathge, and U. Jumar, "Design methodology for high efficient inductive power transfer systems with high coil positioning flexibility," *IEEE Transactions on Industrial Electronics*, Vol. 60, 372–381, 2013.
23. Lu, S., C. Xu, R.-Y. Zhong, and L. Wang, "A RFID-enabled positioning system in automated guided vehicle for smart factories," *Journal of Manufacturing Systems*, Vol. 44, 179–190, 2017.
24. Huang, S.-J., T.-S. Lee, W.-H. Li, and R.-Y. Chen, "Modular on-road AGV wireless charging systems via interoperable power adjustment," *IEEE Transactions on Industrial Electronics*, Vol. 66, 5918–5928, 2019.